JACS
JOURNAL OF THE AMERICAN CHEMICAL SOCIETY

Communication

pubs.acs.org/JACS

Transformation of Ag Nanowires into Semiconducting $AgFeS_2$ Nanowires

Beniamino Sciacca,[†] Anil O. Yalcin,[‡] and Erik C. Garnett*[,†]

[†]Center for Nanophotonics, FOM Institute AMOLF, Science Park Amsterdam 104, 1098 XG Amsterdam, The Netherlands
[‡]Kavli Institute of Nanoscience, Delft University of Technology, Lorentzweg 1, 2628 CJ Delft, The Netherlands

Supporting Information

ABSTRACT: We report on the synthesis of semiconducting $AgFeS_2$ nanowires, obtained from the conversion of Ag nanowires. The study of the conversion process shows that the formation of Ag_2S nanowires, as an intermediate step, precedes the conversion into $AgFeS_2$ nanowires. The chemical properties of $AgFeS_2$ nanowires were characterized by X-ray diffraction, scanning electron microscopy, and energy dispersive X-ray spectroscopy at intermediate steps of the conversion process and show that the temperature at which the reaction takes place is critical to obtaining nanowires as opposed to nanotubes. Optical measurements on nanowire ensembles confirm the semiconducting nature of $AgFeS_2$, with a direct band gap of 0.88 eV.

Ternary I-III-VI_2 semiconductors are receiving increasing attention as promising materials for photovoltaics because of their large absorption coefficient, tunable direct band gap, high conversion efficiency, and low toxicity.[1−6] Copper indium gallium selenide (CIGS)-based solar cells with an efficiency of 21.7% have achieved the record efficiency for single junction polycrystalline material.[7] The outstanding conversion efficiency achieved by I-III-VI_2-semiconductor-based solar cells has motivated us to investigate materials with the chalcopyrite ($CuFeS_2$) structure,[8,9] where the group III element is substituted with Fe.

Nanowire photovoltaics offer several advantages over thin-film architectures including relaxation of lattice strain at heterojunction interfaces[10−15] and strong absorption arising from tunable optical resonances.[16−18] Nanoscale optical resonances maximize absorption in small volumes via antenna effects, which theoretically enables higher open circuit voltage and thus efficiency values, due to reduced bulk recombination and optical concentration.[19,20] Furthermore, at the nanoscale certain chemical processes such as galvanic replacement,[21,22] cation exchange,[23−27] and the Kirkendall effect[28−31] occur much more readily, facilitating the synthesis of complex nanostructures.

$AgFeS_2$ (lenaite) has been recently proposed as a potential absorbing material for solar cells,[32] and in the only report available in literature, its band gap has been reported to be around 1.2 eV. However, to the best of our knowledge, the synthesis of only small $AgFeS_2$ nanocrystals (≈15 nm)[32] or large microparticles[9] has been reported thus far. Here we demonstrate the synthesis of $AgFeS_2$ nanowires, via a solution phase conversion of metallic Ag nanowires into semiconducting $AgFeS_2$ nanowires. X-Ray diffraction (XRD), scanning electron microscopy (SEM), and energy dispersive X-Ray spectroscopy (EDS) characterizations give insight into the conversion mechanism. We also show optical absorption measurements to determine the band gap.

The route to obtain $AgFeS_2$ nanowires was adapted from the previously described synthesis of pure phase FeS_2 nanocrystals.[33] Briefly, $AgFeS_2$ nanowires were obtained by reacting Ag nanowires with iron chloride, sodium thiosulfate, and thioglycolic acid in dimethyl sulfoxide and water at 150 °C.

Representative elemental distributions (Fe, S, and Ag) in a $AgFeS_2$ nanowire measured by EDS are presented in Figure 1a. The full EDS spectrum is shown in Figure S2c. EDS shows that substantial amounts of sulfur and iron are present in the nanowires, along with silver, and they are homogeneously distributed. This indicates that during the conversion process Fe and S diffuse within the nanowire. However, the SEM image in Figure 1a shows the presence of several crystallites in the nanowires, suggesting that they are not single crystalline as opposed to the Ag nanowires employed as precursor. The inset shows a selected area electron diffraction (SAED) pattern confirming the polycrystallinity of these nanowires. Due to the large nanowire diameter, the crystallite size is not entirely clear in transmission electron microscopy images (Figure S1). However, an average crystallite size of 35 nm is obtained using the Scherrer equation (details in SI).

The change of the dispersion color from beige to black (Figure 1b) suggests the formation of a small band gap semiconductor after the conversion process, interestingly preserving the nanowire appearance. This is demonstrated in Figure 1c, that shows a Tauc plot of a $AgFeS_2$ nanowire ensemble deposited on quartz and measured between 0.5 and 1.1 eV. The linear relationship near the band edge indicates a direct band gap, and the intercept value indicates a magnitude of 0.88 eV. Note that the sub-bandgap absorption can be caused either by tail states or by the presence of an indirect transition at smaller energy. Considering the average crystallite size of 35 nm, quantum confinement effects can be excluded in our $AgFeS_2$ nanowires.

The band gap measured is lower than the value of 1.2 eV previously reported on small nanocrystals.[32] The discrepancy in the band gap value measured for our $AgFeS_2$ nanowires compared to that measured for the 15 nm $AgFeS_2$ nanocrystals

Received: February 25, 2015
Published: March 26, 2015

DOI: 10.1021/jacs.5b02051
J. Am. Chem. Soc. 2015, 137, 4340−4343

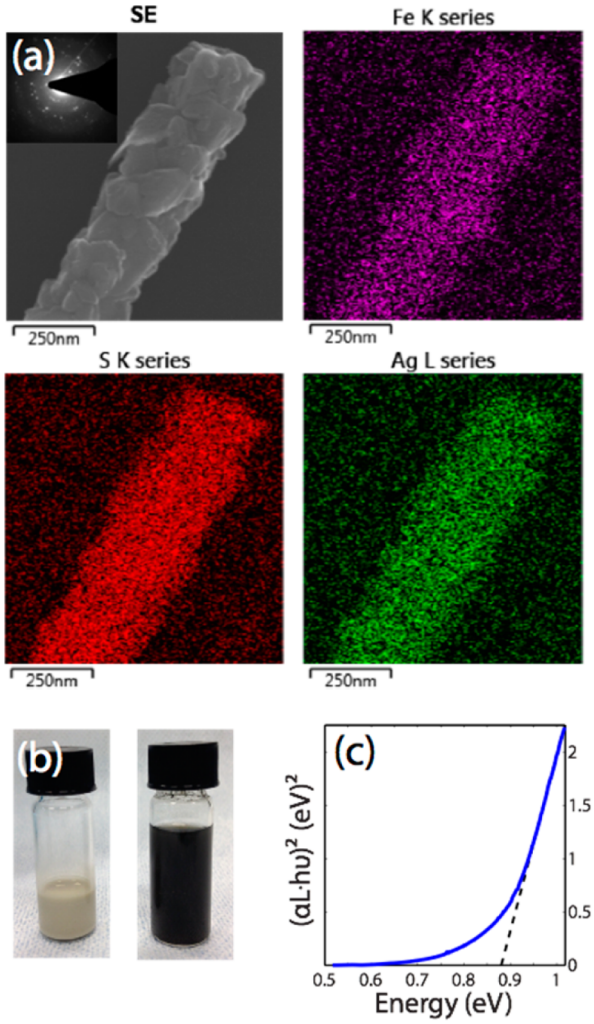

Figure 1. (a) EDS map of $AgFeS_2$ nanowires; the images show the chemical composition, highlighting the homogeneous element distribution within the nanowire. Inset: SAED of $AgFeS_2$ nanowires; the image shows that the nanowires are polycrystalline. (b) Optical images of dispersions of Ag (left) and $AgFeS_2$ (right) nanowires, showing the light absorption properties of $AgFeS_2$. (c) Band gap measurements of $AgFeS_2$ nanowire ensemble drop-cast from solution on a quartz slide; the direct optical transition is around 0.88 eV.

might be due to quantum confinement in the nanocrystals, although there is no report of the Bohr radius for this material. A Bohr radius as large as 10 nm was previously reported for other chalcogenides materials such as $CuInSe_2$;[34] assuming comparable values for $AgFeS_2$, some weak quantum confinement in 15 nm nanocrystals could be expected. However, it is difficult to provide a conclusive explanation, considering the lack of reports in literature about the $AgFeS_2$ band gap.

The conversion of Ag nanowires into $AgFeS_2$ nanowires as a function of the reaction time and temperature was studied. Aliquots of the reacting solution were withdrawn at several time intervals and analyzed by EDS, XRD, and SEM. At $t = 0$, i.e., after mixing the reagent together but before placing them in the heating bath, the nanowires present in the solution are pure crystalline Ag nanowires (Figure 2a,b); no other crystal phases are detectable in the XRD data, although negligible traces of sulfur were detected in the EDS spectrum of nanowires at $t = 0$ (see Figure S2a). This is probably due to residue from the solution or to a thin amorphous silver sulfide layer. This

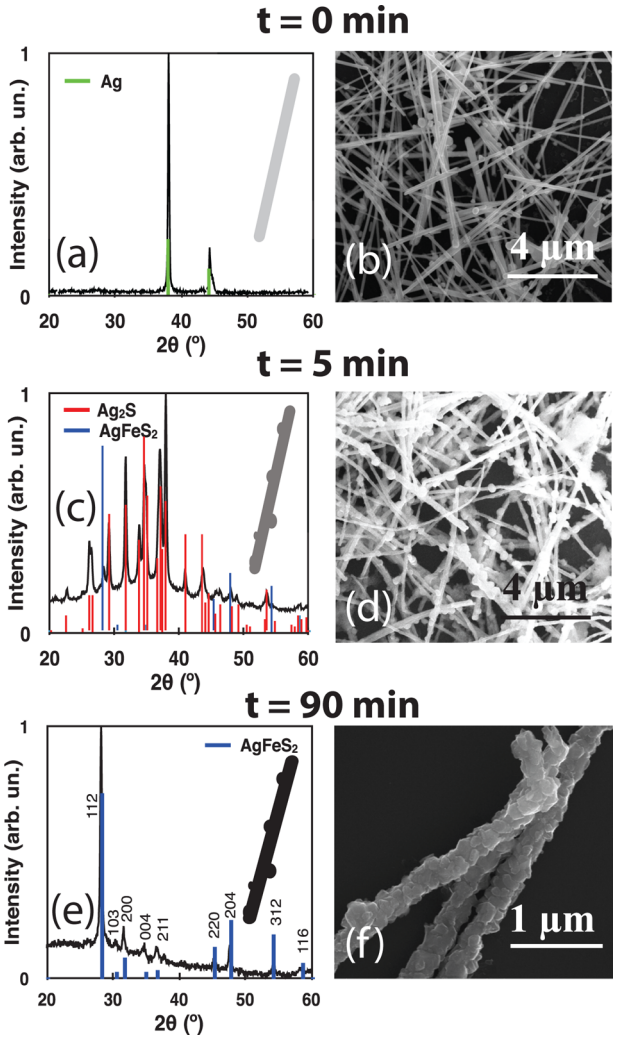

Figure 2. (a) XRD and (b) SEM measurements of an aliquot at $t = 0$. (c) XRD and (d) SEM measurements of the Ag_2S intermediate ($t = 5$ min). (e) XRD and (f) SEM of $AgFeS_2$ nanowires ($t = 90$ min).

suggests that no substantial sulfurization process takes place before heating. After 5 min Ag nanowires are fully converted to Ag_2S nanowires. This is supported by XRD measurements in Figure 2c, showing that the reflection peaks match with those of the achantite (Ag_2S) reference. The SEM image in Figure 2d displays the nanowire geometry of the sample after 5 min, showing changes in the morphology. In particular, a change in morphology is observed in some sections of the nanowires, because of the reorganization of the crystal structure from fcc (Ag) to monoclinic (Ag_2S). Note that at this stage of the conversion process, a small amount of a $AgFeS_2$ phase (peaks aligned with blue lines in Figure 2c) is already present in the sample; this is supported by traces of Fe in the EDS spectrum (see Figure S2b). These findings suggest that the conversion of Ag nanowires to $AgFeS_2$ nanowires goes through an intermediate step, where the formation of Ag_2S nanowires takes place at the very early stage ($t < 5$ min). Thiosulfate disproportionation (eq 1)[35] leads to the formation of H_2S, which sulfurizes Ag nanowires according to eq 2:

$$S_2O^{2-}_{3(l)} + H_2O_{(l)} \xrightarrow{-SO^{2-}_{4(l)}} HS^-_{(l)} + H^+_{(l)} \rightarrow H_2S_{(l)} \quad (1)$$

DOI: 10.1021/jacs.5b02051
J. Am. Chem. Soc. 2015, 137, 4340−4343

$$2Ag_{(s)} + H_2S_{(l)} \xrightarrow{-H_{2(g)}} Ag_2S_{(s)} \quad (2)$$

After the formation of Ag_2S nanowires, H_2S further reacts with Ag_2S and with Fe^{2+} cations, leading to the incorporation of Fe inside the nanowire structure. A possible reaction pathway is shown in eq 3:

$$\overset{\text{I}\ \ -\text{II}}{Ag_2S_{(s)}} + \overset{\text{II}}{2Fe^{2+}_{(l)}} + \overset{\text{I}\ \ -\text{II}}{3H_2S_{(l)}} \xrightarrow[0]{\overset{\text{I}}{-4H^+_{(l)}}} \overset{\text{I}\ \ \text{III}\ -\text{II}}{2AgFeS_{2(s)}} \quad (3)$$
$$-H_{2(g)}$$

No change in the oxidation states of Ag or S is occurring in eq 3, which remain in the I and −II oxidation states, respectively, consistently with what is observed in $CuFeS_2$.[36,37] Iron(II) is oxidized to iron(III), with the concurrent reduction of hydrogen (eq 3). XRD data on nanowire ensembles drop-cast from solution after 90 min are presented in Figure 2e, along with the reference pattern for $AgFeS_2$, reported for comparison. The agreement between the reference pattern and the experimental spectrum is good, demonstrating a successful conversion of Ag nanowires into pure phase crystalline $AgFeS_2$ nanowires.

Note that the shape of the nanowires is preserved at the end of the conversion (Figure 2f), but the roughness of the final samples suggests polycrystallinity. This is consistent with what was observed after 5 min, probably due to the crystal reorganization during the conversion to Ag_2S in the intermediate step. Note that no significant changes in the XRD spectrum are observed after aging for over two months in ambient conditions (see Figure S3).

The effect of the reaction temperature on the conversion process was systematically studied as well, keeping the reaction time at 90 min. If the reaction temperature is too low ($T < 70$ °C), only a sulfurization of the outer surface of Ag nanowires occurs (see Figure S4). XRD measurements (Figure S4a) imply that the main crystalline phase present is Ag. However, EDS shows that a small amount of sulfur is present in the nanowires (see Figure S4b). This suggests that a thin layer of Ag_2S may be formed at the outer surface of Ag nanowires, but not enough to give appreciable X-ray signal, or it could be in an amorphous phase. This is corroborated by the SEM image in Figure S4c, which shows that the surface roughness of the nanowires is increased as compared to freshly prepared Ag nanowires. No traces of Fe are present in the EDS spectrum, suggesting that higher temperatures are needed to promote the Fe incorporation within the nanowire structure. When the reaction is performed at intermediate temperatures (70−120 °C), a hollowing process takes place, leading to the formation of nanotubes, as shown in the backscattered-electron SEM image in Figure S5a. This is probably due to the Kirkendall effect that takes place when the solid-state diffusion rates of flowing inward and outward migrating species are different, resulting in a hollow structure.[28,29] The Kirkendall effect depends also on temperature, geometry, and reagent concentration.[38−40] In our case the disproportionation of thiosulfate occurs faster at higher temperature, leading to an increased concentration of the oxidizing agent (H_2S) and therefore to a larger inward flux. The faster reaction rate and the higher inward flux prevent hollowing at elevated temperatures.

The crystal phase of such nanotubes produced at lower temperatures is a mixture of Ag_2S and $AgFeS_2$, as shown by XRD measurements in Figure S5b. No detectable crystal phase of Ag is present, consistent with migration and oxidation of the Ag core at the surface. EDS spectra confirm as well the presence of Ag, S, and Fe in the nanotubes (see Figure S5c,d).

We have shown a novel synthetic pathway to obtain pure phase $AgFeS_2$ nanowires, employing Ag nanowires as the precursor. The reaction goes through an intermediate step during which Ag_2S nanowires are formed; during this phase the crystal structure undergoes a reorganization due to the different lattices, which produces polycrystalline nanowires. Ag_2S nanowires can then be converted into $AgFeS_2$ nanowires, keeping the same morphology. We have also shown that nanotubes with a mixed phase $Ag_2S/AgFeS_2$ can be prepared by performing the conversion process at a lower temperature. Ensemble optical absorption measurements show that $AgFeS_2$ nanowires have a direct band gap of ∼0.88 eV, which is substantially lower than what was previously reported for $AgFeS_2$ nanocrystals. Given this band gap value, $AgFeS_2$ nanowires could be used for a variety of applications including multiple exciton generation, the bottom cell in a multijunction solar cell, or the low-bandgap layer in a singlet-fission solar cell.

■ ASSOCIATED CONTENT

Supporting Information

Detailed methods and EDS of $AgFeS_2$ and Ag_2S nanowires and $AgFeS_2$ nanotubes are available. This material is available free of charge via the Internet at http://pubs.acs.org.

■ AUTHOR INFORMATION

Corresponding Author

*e.garnett@amolf.nl

Notes

The authors declare no competing financial interest.

■ ACKNOWLEDGMENTS

The authors acknowledge AMOLF technical support, Dr. Bruno Ehrler, Dr. Sarah Brittman for fruitful discussions. We would also like to acknowledge support from the Light Management in New Photovoltaic Materials (LMPV) center at AMOLF. This work is part of the research program of the Foundation for Fundamental Research on Matter (FOM), which is part of The Netherlands Organization for Scientific Research (NWO). The research leading to these results has received funding from the European Research Council under the European Union's Seventh Framework Programme (FP/2007-2013)/ERC grant agreement no. 337328, "NanoEnabledPV".

■ REFERENCES

(1) Yu, L. P.; Kokenyesi, R. S.; Keszler, D. A.; Zunger, A. *Adv. Energy Mater.* **2013**, *3*, 43.

(2) Chirila, A.; Reinhard, P.; Pianezzi, F.; Bloesch, P.; Uhl, A. R.; Fella, C.; Kranz, L.; Keller, D.; Gretener, C.; Hagendorfer, H.; Jaeger, D.; Erni, R.; Nishiwaki, S.; Buecheler, S.; Tiwari, A. N. *Nat. Mater.* **2013**, *12*, 1107.

(3) Chirila, A.; Buecheler, S.; Pianezzi, F.; Bloesch, P.; Gretener, C.; Uhl, A. R.; Fella, C.; Kranz, L.; Perrenoud, J.; Seyrling, S.; Verma, R.; Nishiwaki, S.; Romanyuk, Y. E.; Bilger, G.; Tiwari, A. N. *Nat. Mater.* **2011**, *10*, 857.

(4) Huang, C.; Chan, Y.; Liu, F. Y.; Tang, D.; Yang, J.; Lai, Y. Q.; Li, J.; Liu, Y. X. *J. Mater. Chem. A* **2013**, *1*, 5402.

(5) Wang, D. S.; Zheng, W.; Hao, C. H.; Peng, Q.; Li, Y. D. *Chem. Commun.* **2008**, 2556.

(6) Omata, T.; Nose, K.; Otsuka-Yao-Matsuo, S. *J. Appl. Phys.* **2009**, *105*, 73106.

DOI: 10.1021/jacs.5b02051
J. Am. Chem. Soc. 2015, 137, 4340−4343

(7) Jackson, P.; Hariskos, D.; Wuerz, R.; Kiowski, O.; Bauer, A.; Friedlmeier, T. M.; Powalla, M. *Phys. Status Solidi RRL* **2015**, *9*, 28.
(8) Boon, J. W. *Recl. Trav. Chim. Pays-Bas* **1944**, *63*, 69.
(9) Galembeck, A.; Alves, O. L. *J. Mater. Sci.* **1999**, *34*, 3275.
(10) Schoen, D. T.; Peng, H. L.; Cui, Y. *ACS Nano* **2013**, *7*, 3205.
(11) Tian, B.; Kempa, T. J.; Lieber, C. M. *Chem. Soc. Rev.* **2009**, *38*, 16.
(12) Wu, Y.; Xiang, J.; Yang, C.; Lu, W.; Lieber, C. M. *Nature* **2004**, *430*, 704.
(13) Lauhon, L. J.; Gudiksen, M. S.; Wang, C. L.; Lieber, C. M. *Nature* **2002**, *420*, 57.
(14) Sciacca, B.; Mann, S. A.; Tichelaar, F. D.; Zandbergen, H. W.; van Huis, M. A.; Garnett, E. C. *Nano Lett.* **2014**, *14*, 5891.
(15) Oener, S. Z.; Mann, S. A.; Sciacca, B.; Sfiligoj, C.; Hoang, J.; Garnett, E. C. *Appl. Phys. Lett.* **2015**, *106*, 023501.
(16) Cao, L. Y.; White, J. S.; Park, J. S.; Schuller, J. A.; Clemens, B. M.; Brongersma, M. L. *Nat. Mater.* **2009**, *8*, 643.
(17) Mann, S. A.; Garnett, E. C. *Nano Lett.* **2013**, *13*, 3173.
(18) Garnett, E. C.; Brongersma, M. L.; Cui, Y.; McGehee, M. D. *Annu. Rev. Mater. Res.* **2011**, *41*, 269.
(19) Wallentin, J.; Anttu, N.; Asoli, D.; Huffman, M.; Aberg, I.; Magnusson, M. H.; Siefer, G.; Fuss-Kailuweit, P.; Dimroth, F.; Witzigmann, B.; Xu, H. Q.; Samuelson, L.; Deppert, K.; Borgstrom, M. T. *Science* **2013**, *339*, 1057.
(20) Krogstrup, P.; Jorgensen, H. I.; Heiss, M.; Demichel, O.; Holm, J. V.; Aagesen, M.; Nygard, J.; Morral, A. F. I. *Nat. Photonics* **2013**, *7*, 306.
(21) Oh, M. H.; Yu, T.; Yu, S. H.; Lim, B.; Ko, K. T.; Willinger, M. G.; Seo, D. H.; Kim, B. H.; Cho, M. G.; Park, J. H.; Kang, K.; Sung, Y. E.; Pinna, N.; Hyeon, T. *Science* **2013**, *340*, 964.
(22) Sun, Y. G.; Xia, Y. N. *Science* **2002**, *298*, 2176.
(23) Li, H. B.; Brescia, R.; Povia, M.; Prato, M.; Bertoni, G.; Manna, L.; Moreels, I. *J. Am. Chem. Soc.* **2013**, *135*, 12270.
(24) Beberwyck, B. J.; Alivisatos, A. P. *J. Am. Chem. Soc.* **2012**, *134*, 19977.
(25) Son, D. H.; Hughes, S. M.; Yin, Y. D.; Alivisatos, A. P. *Science* **2004**, *306*, 1009.
(26) Zhang, J. T.; Tang, Y.; Lee, K.; Min, O. Y. *Science* **2010**, *327*, 1634.
(27) Li, H. B.; Zanella, M.; Genovese, A.; Povia, M.; Falqui, A.; Giannini, C.; Manna, L. *Nano Lett.* **2011**, *11*, 4964.
(28) Cummins, D. R.; Russell, H. B.; Jasinski, J. B.; Menon, M.; Sunkara, M. K. *Nano Lett.* **2013**, *13*, 2423.
(29) Gonzalez, E.; Arbiol, J.; Puntes, V. F. *Science* **2011**, *334*, 1377.
(30) Park, J.; Zheng, H.; Jun, Y. W.; Alivisatos, A. P. *J. Am. Chem. Soc.* **2009**, *131*, 13943.
(31) Yin, Y. D.; Rioux, R. M.; Erdonmez, C. K.; Hughes, S.; Somorjai, G. A.; Alivisatos, A. P. *Science* **2004**, *304*, 711.
(32) Han, S. K.; Gu, C.; Gong, M.; Wang, Z. M.; Yu, S. H. *Small* **2013**, *9*, 3765.
(33) Bai, Y. X.; Yeom, J.; Yang, M.; Cha, S. H.; Sun, K.; Kotov, N. A. *J. Phys. Chem. C* **2013**, *117*, 2567.
(34) Zhong, H. Z.; Wang, Z. B.; Bovero, E.; Lu, Z. H.; van Veggel, F. C. J. M.; Scholes, G. D. *J. Phys. Chem. C* **2011**, *115*, 12396.
(35) Pryor, W. A. *J. Am. Chem. Soc.* **1960**, *82*, 4794.
(36) Pearce, C. I.; Pattrick, R. A. D.; Vaughan, D. J.; Henderson, C. M. B.; van der Laan, G. *Geochim. Cosmochim. Acta* **2006**, *70*, 4635.
(37) Goh, S. W.; Buckley, A. N.; Lamb, R. N.; Rosenberg, R. A.; Moran, D. *Geochim. Cosmochim. Acta* **2006**, *70*, 2210.
(38) Hung, L. I.; Tsung, C. K.; Huang, W. Y.; Yang, P. D. *Adv. Mater.* **2010**, *22*, 1910.
(39) Yin, Y. D.; Erdonmez, C. K.; Cabot, A.; Hughes, S.; Alivisatos, A. P. *Adv. Funct. Mater.* **2006**, *16*, 1389.
(40) Fan, H. J.; Gosele, U.; Zacharias, M. *Small* **2007**, *3*, 1660.

DOI: 10.1021/jacs.5b02051
J. Am. Chem. Soc. 2015, 137, 4340−4343